Materials Research Bulletin 44 (2009) 1948–1953

Contents lists available at ScienceDirect

Materials Research Bulletin

journal homepage: www.elsevier.com/locate/matresbu

Manufacture, microstructure and mechanical properties of Mo–W–N nanostructured hard films

J.F. Yang [a], Z.G. Yuan [a], G.G. Zhang [b], X.P. Wang [a], Q.F. Fang [a,b,*]

[a] Key Laboratory of Materials Physics, Institute of Solid State Physics, Chinese Academy of Sciences, Hefei 230031, PR China
[b] Department of Materials Sciences and Engineering, Nanchang Hangkong University, Nanchang 330034, PR China

ARTICLE INFO

Article history:
Received 5 September 2008
Received in revised form 8 June 2009
Accepted 25 June 2009
Available online 4 July 2009

Keywords:
A. Nitrides
A. Thin films
B. Sputtering
C. X-ray diffraction
D. Mechanical properties

ABSTRACT

$Mo_{1-x}W_xN_y$ (x = 0–0.67) hard films were fabricated on wafers of silicon and high speed steel by dc magnetron sputtering technique. The effect of tungsten concentration on the phase composition, microstructure, surface morphology, hardness, adhesion, and corrosion resistance of the films was studied by X-ray diffraction, scanning electron microscopy, nano-indentation, and scratch test. It was found that if the W concentration (x) in the film is in the range of 0–0.52, the films exhibit fcc $(Mo,W)N_y$ single phase where larger W atoms substituted Mo atoms in fcc MoN_y. At higher x values ($x > 0.52$) the films exhibit a two-phase structure consisting of fcc $(Mo,W)N_y$ and pure bcc tungsten phase. The hardness of the $Mo_{1-x}W_xN_y$ films increases at first with increasing x, and then decreases after passing a maximum. The maximum hardness of 47 GPa is obtained at x = 0.37 corresponding to an adhesion strength of 60 N. The Mo–W–N coated high speed steel has a lower corrosion current density and higher corrosion potential than the bare high speed steel substrates.

© 2009 Elsevier Ltd. All rights reserved.

1. Introduction

Over the last decades, coatings of transition metal carbides and nitrides prepared by PVD and CVD techniques have been extensively researched and widely applied as protective coatings for drilling, machining, and cutting tools, owing to their excellent performance in hardness, wear and corrosion resistance [1–4]. In the nitride system, ternary transition metal nitrides have attracted more and more attention because they provide a broader range of nitride structure types for a fine-tuning of mechanical and electrical properties. In ternary systems it is possible to optimize the performance such as hardness, elasticity, thermal expansion coefficient, and corrosion resistance by adjusting the compositions. The most frequently used methods to synthesize the ternary transition metal nitrides are the nitriding of binary alloys [5] and reactive co-sputtering of two different kinds of metals [6–8].

Molybdenum nitride was proved to be a promising candidate providing low friction coefficient and high wear resistance as compared to other nitride systems [1], although its hardness is lower than that of titanium nitride. Further more, it was reported that partial substitution of Mo by other elements such as Al [9,10] can greatly improve the hardness and oxidation resistance of molybdenum nitride films. Tungsten nitride coatings were usually used as barriers and electrodes in optical and microelectronic fields due to their high stability and excellent conductivity properties [1]. Nevertheless, few studies were focused on the mechanical properties of W–N coatings [11] or Mo–W–N coatings [12].

In this study, the co-sputtering of molybdenum and tungsten by dc magnetron sputtering technique was exploited to synthesize nanostructured ternary Mo–W–N hard films on the substrates of silicon and high speed steel, in order to investigate the effect of the addition of W in Mo–N nitride on the properties of Mo–W–N films. Microstructure and surface morphology of the nanostructured coatings were analyzed using SEM and XRD techniques. Microhardness, adhesion and corrosion resistance of the coatings were also investigated.

2. Experimental procedure

The Mo–W–N hard films were sputter-deposited onto substrates of high speed steel (W18Cr4V) coins and Si(1 1 1) wafers in an atmosphere of Ar + N_2 using dc magnetron sputtering technique with a W(99.9%) + Mo(99.9%) composite target. The W/Mo composite target was manufactured by fixing a sheet of molybdenum with thickness of 2 mm to the surface of tungsten target with diameter of 60 mm. By regulating the surface area of the molybdenum sheet, the atomic ratio of Mo to W in the films can be controlled conveniently.

* Corresponding author at: Key Laboratory of Materials Physics, Institute of Solid State Physics, Chinese Academy of Sciences, POB 1129, Hefei 230031, PR China. Tel.: +86 551 5591459; fax: +86 551 5591434.
E-mail address: qffang@issp.ac.cn (Q.F. Fang).

0025-5408/$ – see front matter © 2009 Elsevier Ltd. All rights reserved.
doi:10.1016/j.materresbull.2009.06.013

The films were coated on silicon wafers for composition, microstructure and hardness analysis. For the analysis of adhesion and corrosion resistance property, the films were deposited on coins of high speed steel. These coins of high speed steel with diameter of 12 mm and thickness of 2 mm were polished by different sand paper and diamond abrasive pastes. All substrates were ultrasonically cleaned using a mixture of acetone and alcohol, rinsed in deionized water, dried in a nitrogen jet, and then immediately introduced into the vacuum chamber. The substrate was fixed to the tilted substrate holder with a distance of about 55 mm away from the target. The substrate was electrically grounded.

The vacuum chamber was firstly pumped down to 7.0×10^{-4} Pa and then the substrate was heated up to 500 °C. The Ar and N_2 were introduced into the chamber at a rate of 40 and 30 sccm as plasma and reactive gas sources, respectively. The working pressure after gas input was controlled as 1.0 Pa. The input power of the target was fixed at 120 W.

The crystallographic phases of the coatings were determined by grazing incidence X-ray diffraction (Philips X'pert PRO MPD) in the scanning range from 30° to 90° with a step of 0.06°, using monochromatized Cu Kα radiation operating at 40 kV and 40 mA. The cell parameters of the deposited films were evaluated by the whole pattern refinement of the XRD patterns using the fullprof program [13].

The surface and cross-section morphology of coatings were characterized with a field-emission scanning electron microscope (FESEM, Sirion 200, FEI). The elemental composition of films, that is, the values of x and y in $Mo_{1-x}W_xN_y$, was determined by energy dispersive spectroscopy (EDS) equipped in FESEM. The thickness of all coatings is determined by measuring the cross-section of the as-deposited films with FESEM and the deposition rate was obtained through dividing the thickness by deposition time. Table 1 lists the elemental composition and deposition rate of $Mo_{1-x}W_xN_y$ films at various x value. It was found that the corresponding deposition rates for $Mo_{1-x}W_xN_y$ films with $x = 0$, 0.11, 0.23, 0.37, 0.52, 0.59, 0.67 were 0.45, 0.42, 0.43, 0.44, 0.40, 0.43, and 0.41 nm/s, respectively. The addition of W in Mo–N films leads to slight reduction in deposition rate of Mo–N films.

The microhardness and Young's modulus of the coatings were analyzed with a nano-indenter apparatus (MTS NANO Indenter® G200) at room temperature. In the hardness measurements, the penetration depth was kept at about 10% of the film thickness in order to exclude the possible effects of substrate and the surface roughness of films. The data of hardness and Young's modulus were averaged from nine indentation tests for each sample to improve measurement accuracy.

Adhesion strength (critical load, L_c) of the film to the substrate was measured with a scratch tester (WS-2005 equipped with an acoustic emission detector) by increasing load from 0 to 100 N at a loading rate of 50 N/min. The standard diamond Rockwell C indenter tip of 200 μm in radius was used. The scratch length was fixed as 10 mm and the scratch rate as 5 mm/min.

Table 1
The elemental composition and deposition rate of $Mo_{1-x}W_xN_y$ films with various x values.

W/(W + Mo) (at.%)	Elemental composition	Deposition rate (nm/s)
0	Mo49N51	0.45
11	Mo46W6N48	0.42
23	Mo43W13N44	0.43
37	Mo37W22N41	0.44
52	Mo31W34N35	0.40
59	Mo28W40N32	0.43
67	Mo24W49N27	0.41

The potentiodynamic study was carried out at a scanning rate of 1 mV/s using a model 273A potentiostat/galvanostat device (EG&G Princeton Applied Research) in a typical three-electrode arrangement with the coated sample as working electrode, a 1 cm^2 platinum plate as the counter electrode, and a saturated calomel electrode as the reference electrode. The aqueous corrosion behavior of the coated steels was measured in a solution of 3.5 wt.% sodium chloride at room temperature. The sides of specimens except for the area of interest were sealed with epoxy resin.

3. Results and discussion

3.1. Structure

Fig. 1 shows the X-ray diffraction (XRD) patterns of the various $Mo_{1-x}W_xN_y$ films deposited on silicon at 500 °C in $Ar + N_2$ atmosphere with x values in the range of 0–67 at.%. Pure Mo–N films deposited without tungsten exhibits the typical fcc NaCl structure with the presence of (1 1 1), (2 0 0), (2 2 0), (3 1 1), and (2 2 2) diffraction peaks at diffraction angles around 37°, 43°, 62°, 75° and 79°, respectively. For $Mo_{1-x}W_xN_y$ films with $x \leq 52\%$, the structure is still fcc NaCl structure. In films with $x > 52\%$ however, a two-phase structure was detected: a fcc NaCl-type phase and a bcc W phase, which is confirmed by the appearance of additional peaks at diffraction angles around 40°, 73° and 87° for film with $x = 59\%$ and peaks at diffraction angles around 40°, 58°, 73°, and 87° for film with $x = 67\%$, respectively. These additional peaks are the (1 1 0), (2 0 0), (2 1 1), and (2 2 0) diffraction peaks of bcc W phase, respectively. The two-phase structure of fcc W_2N and bcc W was also observed in W–N and W–Ti–N systems [14,15].

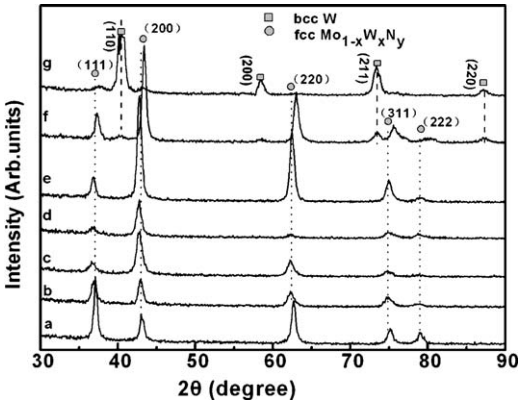

Fig. 1. XRD patterns of $Mo_{1-x}W_xN_y$ films with different x values: (a) 0, (b) 0.11, (c) 0.23, (d) 0.37, (e) 0.52, (f) 0.59, (g) 0.67.

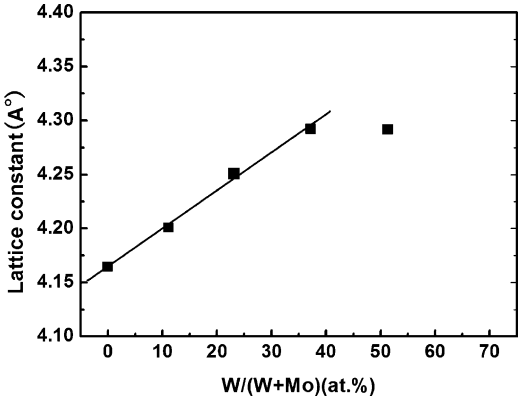

Fig. 2. The evolution of lattice constant of fcc $Mo_{1-x}W_xN_y$ phase as a function of W concentration (x).

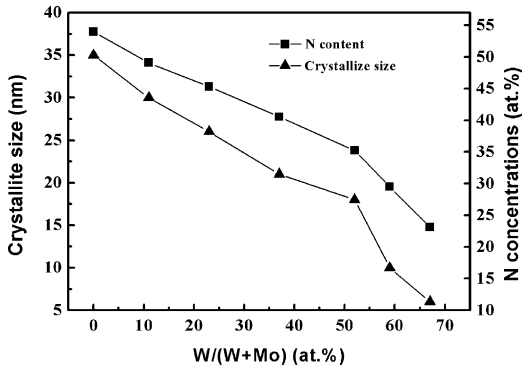

Fig. 3. Tungsten concentration (x) dependence of crystallite size and nitrogen concentration (y) in $Mo_{1-x}W_xN_y$ films.

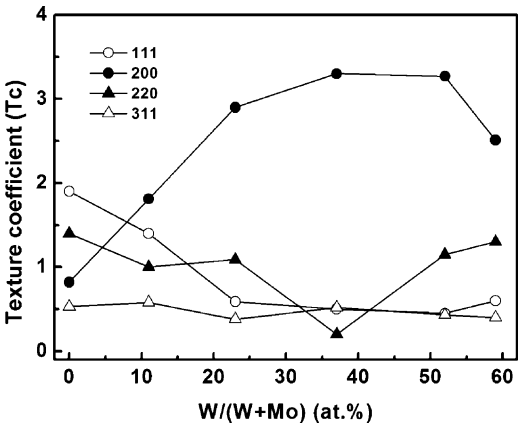

Fig. 4. Variation of texture coefficient of $Mo_{1-x}W_xN_y$ films with tungsten concentration (x).

The lattice constant of fcc phase calculated from the whole pattern refinement is shown in Fig. 2. As the tungsten concentration (x) increases from 0 to 37 at.% the lattice constant increases linearly, which obeys the Vegard law and suggests that single phase of fcc (Mo,W)N_y was formed where the larger tungsten atoms substitute smaller molybdenum atoms in fcc MoN_y phase. However, at $x = 0.52$, the variation of lattice constant deviate from the Vegard law, which is often happened when W substitutes Mo to form doped compounds [16,17], where the decrease of lattice constant at high doping content was explained as the decrease in coordination number around W [17]. It should be pointed out that the lattice constant of fcc (Mo,W)N_y phase at higher tungsten concentration ($x > 0.52$) was not calculated owing to the appearance of bcc W phase.

The appearance of bcc W phase in films with higher tungsten contents is due to the reduction of nitrogen concentration in films, as indicated in Table 1 and more clearly in Fig. 3, where the content of nitrogen in the films deduced from the EDS data decreases monotonously with increasing tungsten content. In the pure Mo–N film ($x = 0$) the content of nitrogen is about 51 at.%, implying the over-stoichiometry in fcc Mo_2N phase. When $x = 0.52$ the content of nitrogen is about 35% that corresponds nearly to the stoichiometry of fcc structured $(Mo_{0.48}W_{0.52})_2N$. The content of nitrogen reaches 27 at.% at $x = 0.67$, where bcc W phase appears. The decrease of nitrogen with increasing W contents can be understood as the lower chemical affinity of N to W than to Mo [18].

As shown in Fig. 3, the crystallite size calculated from the width of XRD peaks by Debye–Scherrer equation is about 38 nm for pure Mo–N film and decreases monotonously to about 18 nm when the W content (x) is about 52%. This is reasonable because competition between nucleation and grain growth exists during the whole deposition process and nitrogen deficiency would retard the process of grain growth [4]. For films with two-phase structure ($x = 0.59$ and 0.67), crystallite size sharply decreases to 5–8 nm, since the existence of bcc W phase in the Mo–W–N coatings will impede the grain growth of fcc (Mo,W)N_y crystallites.

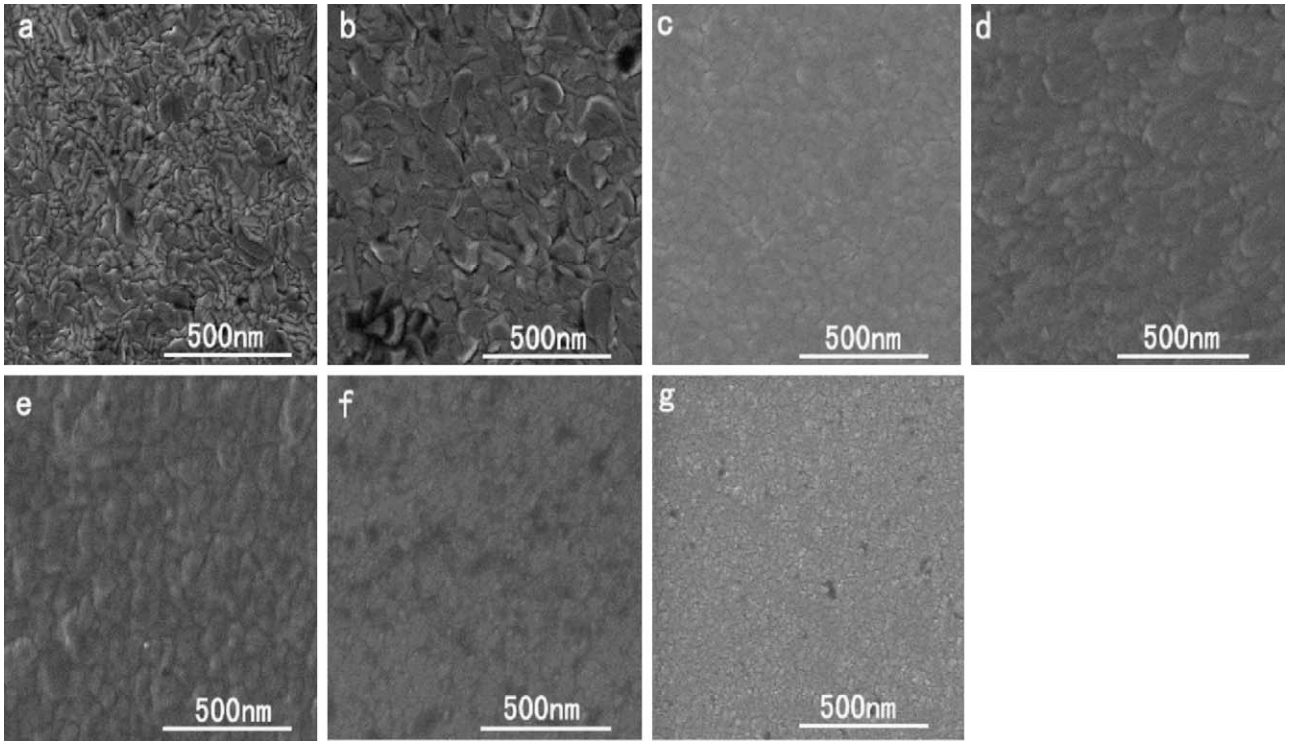

Fig. 5. FESEM surface morphology of $Mo_{1-x}W_xN_y$ films with different x values: (a) 0, (b) 0.11, (c) 0.23, (d) 0.37, (e) 0.52, (f) 0.59, (g) 0.67.

The effect of W concentration on the coating texture can be better demonstrated using the texture coefficient $T_c(h\,k\,l)$ [19,20], as plotted in Fig. 4. Corresponding to the decrease of texture coefficients for the ⟨1 1 1⟩ reflections, the texture coefficients of ⟨2 0 0⟩ increase gradually from 0.91 to 3.21 with the increase of x value from 0 to 0.37, which indicates that the texture of the $Mo_{1-x}W_xN_y$ films evolves from (1 1 1) to (2 0 0). Yau et al. [21] have investigated the texture change of tungsten doped chromium nitride films and reported that the preferential orientation of Cr–W–N films changes from (1 1 1) to (2 0 0) due to the open channeling direction effect of (1 0 0). Multman et al. [22] and Zeitler et al. [23] have investigated the texture dependence of TiN films on incident ion/atom flux, and pointed out that at normal incidence the (1 1 1) plane presents a dense array of atoms and [1 0 0] is the most open channeling direction. Alireza et al. have observed the same trend of texture evolution in the Ti–Ni–N system [24]. In this study, the fcc structure of $Mo_{1-x}W_xN_y$ films is similar to that of $Cr_{1-x}W_xN_y$ and Ti–Ni–N films. An increasing number of Mo atoms were replaced by W atoms through the open channeling direction.

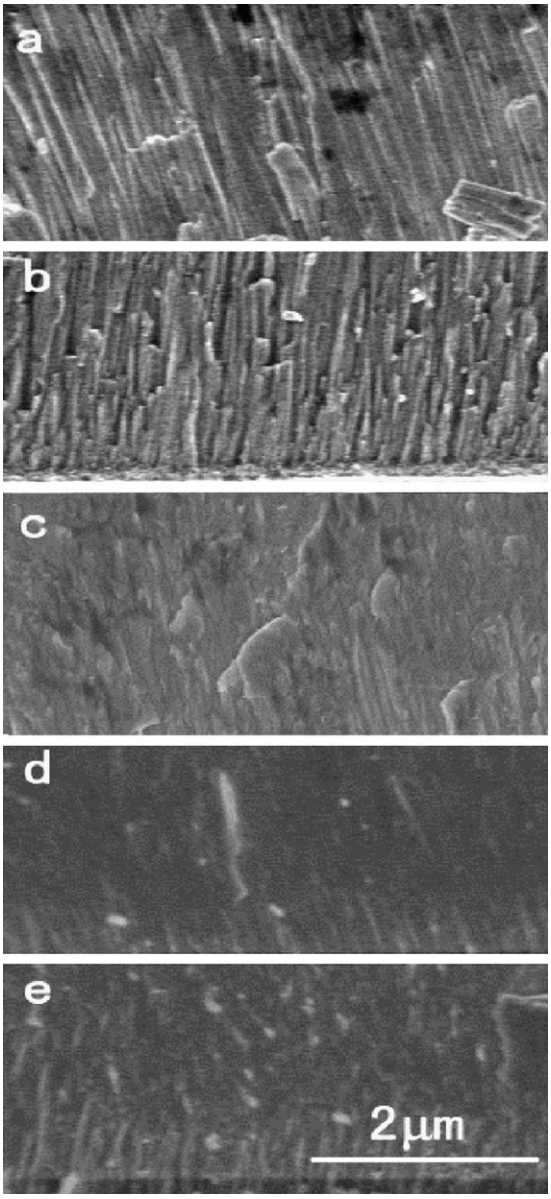

Fig. 6. FESEM cross-sectional micrographs of $Mo_{1-x}W_xN_y$ films with different x values: (a) 0, (b) 0.11, (c) 0.23, (d) 0.37, (e) 0.52.

3.2. Surface morphology

The FESEM images of Mo–W–N films deposited on high speed steel substrates at 500 °C with different W content (x) are presented in Fig. 5. It can be seen that pure Mo–N film (Fig. 5a) has a coarse surface with a few cavities. The surface becomes denser when 11 at.% W was added and cavities disappear (Fig. 5b). With further addition of W, the surface becomes more compact and smoother. When x = 0.37 and 0.52 (Fig. 5d and e), a densely compacted surface was obtained.

The effect of W concentration on the cross-sectional morphology of $Mo_{1-x}W_xN$ films is shown in Fig. 6. When x = 0 and 0.11, the $Mo_{1-x}W_xN_y$ films show a typical columnar structure (Fig. 6a and b) and the average columnar width is about 240 and 200 nm, respectively. The decrease of columnar grain size with increasing W content is in accordance with the decrease of grain size deduced from XRD results. When x = 0.23 the film has a very dense structure with very fine grains and dense grain boundaries (Fig. 6c). With the further addition of tungsten (x = 0.37 and 0.52) the films show a smooth and glassy appearance as shown in Fig. 6d and e, and the columnar grain size sharply decreases to about 20–50 nm.

3.3. Hardness

Fig. 7a represents the variation of hardness and elastic modulus of the films as a function of W concentration (x). In contrast to the gradual decrease of the average grain size with increasing W concentration as shown in Fig. 3, the hardness and elastic modulus of films firstly increase to a maximum of 47 and 586 GPa at x = 0.37 and then dramatically decrease to 19 GPa and 210 GPa at x = 0.67.

The hardness enhancement could be attributed to the combined effect of solid solution strengthening, grain refinement,

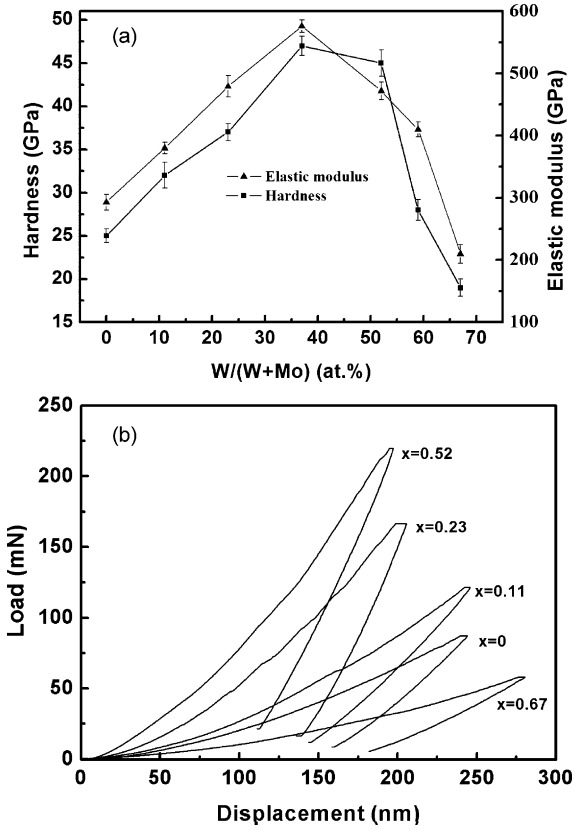

Fig. 7. (a) Hardness and elastic modulus of $Mo_{1-x}W_xN_y$ films as a function of tungsten content; (b) load–displacement curves of $Mo_{1-x}W_xN_y$ films with different tungsten content.

densely compacted morphology, and possibly the macroscopic compressive stress in the films. It was reported that the substitution of host atoms by larger impurity atoms induces compressive strain in the surrounding crystal lattice [25] and thus results in higher hardness. The hardness decreases with decreasing grain size in the two-phase structured Mo–W–N films, because the weakening effect of comparatively softer W phase surpasses the strengthening effect of finer grains. It was reported in the Mo–Ag–N, Cr–Ag–N and Ti–Ni–N systems that the presence of a large amount of softer component facilitates the grain boundary sliding, leading to the decrease of hardness [24,26,27].

As well known, the toughness of films can be expressed qualitatively by the elastic recovery (W_e), which was defined as the ratio of the recovery displacement after unloading to the total indentation displacement [28]. The elastic recovery of $Mo_{1-x}W_xN_y$ films calculated from the corresponding load–displacement curves shown in Fig. 7b are 34% ($x = 0$), 41% ($x = 0.11$), 32% ($x = 0.23$), 43% ($x = 0.52$), and 35% ($x = 0.67$), respectively. These values of W_e are much lower than that of amorphous CN films (70–90%) [29], indicating good toughness of $Mo_{1-x}W_xN_y$ films.

3.4. Adhesion strength

Fig. 8 shows the evolution of critical load (L_c) as a function of W contents for Mo–W–N films deposited on high speed steel substrate. The inset depicts the scratch test results for a $Mo_{1-x}W_xN_y$ ($x = 0.37$) film deposited on high speed steel substrate, indicating adhesion strength of 60 N. It can be seen that the adhesion strength of pure Mo–N films is about 25 N. With increasing tungsten concentration, the adhesion strength of $Mo_{1-x}W_xN_y$ films increases linearly and reach a maximum of 60 N at $x = 0.37$, and then decreases linearly to a value of 37 N at $x = 0.67$. The reason why the adhesion strength exhibits a maximum at $x = 0.37$ is presently unknown.

The increase of adhesion strength can be attributed to the lower concentration gradient between high speed steel (W18Cr4V) substrate and films due to the increase of W content in the films, and densely compacted microstructure. However, the decrease in adhesion strength at higher W concentration can be explained by the formation of metallic tungsten phase that degrades the overall integrity of Mo–W–N films, similar to the results reported in the Cr–Ag–N and Cr–W–N systems [24].

3.5. Corrosion behavior

W–Mo–N coatings exhibit improvement in corrosion resistance in comparison with uncoated high speed steel substrates, as shown

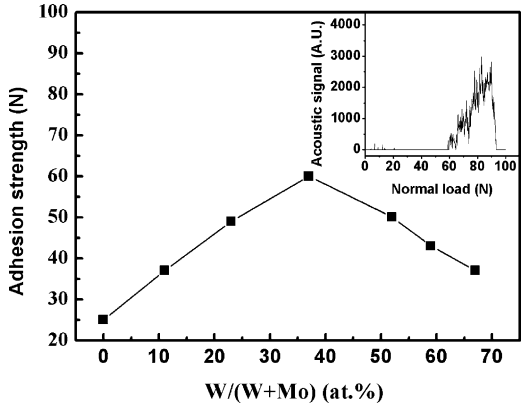

Fig. 8. Adhesion strength of $Mo_{1-x}W_xN_y$ films deposited on high steel substrates as a function of tungsten content. The inset depicts the scratch test results for a $Mo_{1-x}W_xN_y$ ($x = 0.37$) film.

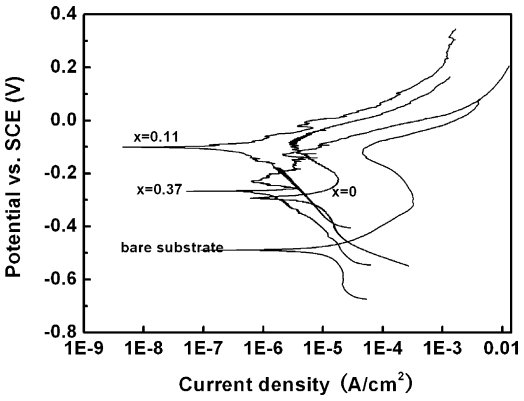

Fig. 9. Potentiodynamic polarization curves for bare and $Mo_{1-x}W_xN_y$ coated high speed steel substrates.

in Fig. 9. The free corrosive potential (E_{corr}) changes greatly due to the W–Mo–N coating on the high speed steel substrates, which is about −0.5 V for uncoated, −0.3 V for pure MoN_y coated, −0.1 V for $Mo_{1-x}W_xN_y$ ($x = 0.11$ and 0.37) coated high speed steel, respectively. The corresponding free corrosive current (I_{corr}) is about 16.3, 7.2, 0.6, and 0.8 μA, respectively.

The rather low corrosion potential (E_{corr}) and high corrosion current density (I_{corr}) values imply that the uncoated high speed steel substrate has poor corrosion resistance to the tested condition. In contrast, the Mo–W–N films show higher corrosion potential and lower corrosion current than Mo–N films, indicating good corrosion resistance of Mo–W–N composite coatings to the tested condition.

4. Conclusions

Mo–W–N nanostructured hard films were fabricated using dc magnetron sputtering technique at the same deposition condition. The W content was controlled through adjusting the area ratio of molybdenum sheet to tungsten target. The results of this study can be concluded as follows:

(1) The nitrogen concentration and the crystallite size of the $Mo_{1-x}W_xN_y$ films decrease monotonously with increasing W content (x).
(2) When $x \leq 0.52$ the Mo–W–N films exhibit a fcc $(Mo,W)N_y$ phase. When $x > 0.52$ however, a two-phase structure appears: fcc $(Mo,W)N_y$ phase and bcc W phase.
(3) The maximum hardness of approximately 47 GPa was obtained for the $Mo_{1-x}W_xN_y$ films at $x = 0.37$. For films with two-phase structure, the hardness decreased to 19 GPa in spite of the smaller crystallite size of 6 nm.
(4) The adhesion strength increased at first from 25 to 60 N and then decreased to below 40 N with increasing W content.
(5) The lower corrosive current and higher corrosive potential of Mo–W–N coatings on high speed steel in a solution of 3.5 wt.% sodium chloride illustrate good corrosion resistance and adequate protective effect of the $Mo_{1-x}W_xN_y$ films.

Acknowledgments

This work has been subsidized by the National Natural Science Foundation of China (Grant Nos. 50672100, 50702061, 10874185), and the Aeronautic Science Foundation (Grant No. 20071656004).

References

[1] L.E. Toth, Transition Metal Carbides and Nitrides, Academic Press, New York, 1971
[2] H. Holleck, J. Vac. Sci. Technol. A 4 (1986) 2661.
[3] T. Hurkmans, T. Trinh, D.B. Lewis, Surf. Coat. Technol. 76–77 (1995) 159.

[4] P. Hones, R. Consiglio, N. Randall, Surf. Coat. Technol. 125 (2000) 179.
[5] R.M. Ibberson, R. Cywinski, Physica B 180/181 (1992) 329.
[6] R. Saha, R.B. Inturi, J.B. Barnard, Surf. Coat. Technol. 82 (1996) 42.
[7] C. Wiemer, R. Sanjines, F. Levy, Surf. Coat. Technol. 86/87 (1996) 372.
[8] P. Panjan, B. Navinsek, A. Cvelbar, Thin Solid Films 282 (1996) 298.
[9] J.F. Yang, Q. Liu, X.P. Wang, Mater. Res. Bull. 44 (2009) 86.
[10] J. Šůna, J. Musil, P. Dohnal, Vacuum 80 (2006) 588.
[11] T. Yamamoto, M. Kawate, H. Hasegawa, Surf. Coat. Technol. 193 (2005) 372.
[12] S. Song, Y. Liu, M. Li, Microelectron. Eng. 83 (2006) 423.
[13] J. Rodriguez-Carvajal, Physica B 192 (1993) 55.
[14] L. Boukhris, J.M. Poitevin, Thin Solid Films 310 (1997) 222.
[15] P.N. Silvaa, J.P. Diasa, A. Cavaleiro, Surf. Coat. Technol. 200 (2005) 186.
[16] D. Li, X.P. Wang, Q.F. Fang, Phys. Stat. Solidi (a) 204 (2007) 2270.
[17] G. Corbel, Y. Laligant, F. Goutenoire, Chem. Mater. 17 (2005) 4678.
[18] G.V. Samsonov, I.M. Vinitskii, Handbook of Refractory Compounds, New York, 1980.
[19] M.I. Jones, I.R. McColl, D.M. Grant, Surf. Coat. Technol. 132 (2000) 143.
[20] H.E. Cheng, M.H. Hon, J. Appl. Phys. 79 (1996) 8047.
[21] B.-S. Yau, D. Lin, Thin Solid Films 516 (2008) 1877.
[22] L. Multman, W.D. Münz, J. Musil, J. Vac. Sci. Technol. A 9 (1991) 434.
[23] M. Zeitler, J.M. Gerlach, T. Kraus, Appl. Phys. Lett. 70 (1997) 1254.
[24] A. Alireza, P.R. Jean, T. Claude, Surf. Coat. Technol. 200 (2006) 6298.
[25] W.D. Callister, Materials Science and Engineering, John Wiley &Sons, Inc., 2000„ p. 168.
[26] G. Witold, S. Tomasz, Surf. Coat. Technol. 201 (2006) 1469.
[27] S.H. Yao, Y.L. Su, W.H. Kao, Surf. Coat. Technol. 201 (2006) 2520.
[28] W.T. Zheng, H. Sjostrom, I. Ivanov, J. Vac. Sci. Technol. A 14 (1996) 2696.
[29] K.H. Lee, O. Takai, Diam. Relat. Mater. 14 (2005) 1444.